Satellite constraint on the tropospheric ozone radiative effect

A. Rap[1], N. A. D. Richards[1,2], P. M. Forster[1], S. A. Monks[1], S. R. Arnold[1], and M. P. Chipperfield[1,2]

[1]School of Earth and Environment, University of Leeds, Leeds, UK, [2]National Centre for Earth Observation, University of Leeds, Leeds, UK

Abstract Tropospheric ozone directly affects the radiative balance of the Earth through interaction with shortwave and longwave radiation. Here we use measurements of tropospheric ozone from the Tropospheric Emission Spectrometer satellite instrument, together with chemical transport and radiative transfer models, to produce a first estimate of the stratospherically adjusted annual radiative effect (RE) of tropospheric ozone. We show that differences between modeled and observed ozone concentrations have little impact on the RE, indicating that our present-day tropospheric ozone RE estimate of $1.17 \pm 0.03 \, \mathrm{W \, m^{-2}}$ is robust. The RE normalized by column ozone decreased between the preindustrial and the present-day. Using a simulation with historical biomass burning and no anthropogenic emissions, we calculate a radiative forcing of $0.32 \, \mathrm{W \, m^{-2}}$ for tropospheric ozone, within the current best estimate range. We propose a radiative kernel approach as an efficient and accurate tool for calculating ozone REs in simulations with similar ozone abundances.

1. Introduction

Tropospheric ozone plays a key role in climate and is generally recognized as the third most important greenhouse gas after carbon dioxide and methane [*Myhre et al.*, 2013]. As ozone is not a primary emitted species, its abundance and distribution is controlled by atmospheric chemistry and transport. In the troposphere this is largely in situ photochemical oxidation of natural and anthropogenic precursor species, e.g., carbon monoxide, methane, and other volatile organic compounds, in the presence of nitrogen oxides [e.g., *Lelieveld and Dentener*, 2000]. Since the Industrial Revolution emissions of these precursors have increased substantially, leading to an increase in tropospheric ozone concentrations between the preindustrial (PI) and the present-day (PD). Through interaction with both shortwave (SW) and longwave (LW) radiation, this increase in tropospheric ozone concentrations has had a warming effect on climate, with the Intergovernmental Panel on Climate Change (IPCC) current best estimate for its radiative forcing (RF) at $0.4 \, \mathrm{W \, m^{-2}}$, with a 5 to 95% confidence range of (0.2 to $0.6 \, \mathrm{W \, m^{-2}}$) [*Myhre et al.*, 2013]. These estimates are almost entirely based on model simulations, the large associated uncertainty being attributed to the different model formulations and the potential overestimation of PI ozone concentrations [*Myhre et al.*, 2013; *Stevenson et al.*, 2013]. *Bowman et al.* [2013] have proposed an approach based on satellite observations and model simulations, where the intermodel uncertainty is reduced by 30% by correlating biases in modeled outgoing LW radiation to the model ozone RF deviation from the ensemble mean.

The tropospheric ozone radiative effect (RE), similarly to the aerosol RE [*Boucher and Tanré*, 2000; *Rap et al.*, 2013; *Heald et al.*, 2014], is defined as the radiative flux imbalance between the incoming SW solar radiation and the outgoing LW infrared radiation resulting from the presence of all (natural and anthropogenic) tropospheric ozone. For consistency with the RF concept [*Forster et al.*, 2007; *Myhre et al.*, 2013], we calculate this imbalance at the tropopause, after allowing for stratospheric temperatures to readjust to radiative equilibrium. Thus, the RE is different from the more often used RF metric, which is essentially the change in RE over time, usually calculated between the PI and PD. While quantifying the tropospheric ozone RE is important in order to understand the total effect of both natural and anthropogenic tropospheric ozone on climate, existing studies only provide a few monthly mean instantaneous RE (IRE) estimates which differ by a factor of 5. *Joiner et al.* [2009] used a residual approach and measurements from the NASA Aura Ozone Monitoring Instrument and Microwave Limb Sounder to estimate an average January and July 2005 IRE at the tropopause of $1.53 \, \mathrm{W \, m^{-2}}$. In their study they used a uniform ozone profile for SW calculations and a scaled model daily profile for LW calculations. *Worden et al.* [2011] used NASA Aura Tropospheric Emission

Spectrometer (TES) measurements to estimate a LW IRE at the top of the atmosphere (TOA) for August 2006 of $0.33\,\mathrm{W\,m^{-2}}$. The aim of our study is to understand the difference between these two current estimates and to provide the first estimate of the annual mean stratospherically adjusted tropospheric ozone RE.

2. Methodology

We use ozone satellite measurements from TES, together with the TOMCAT chemical transport model and the *Edwards and Slingo* [1996] radiative transfer model to estimate the PD tropospheric ozone RE. The tropopause definition used in this study is the chemical tropopause based on the 150 ppbv ozone level, also used by *Young et al.* [2013]. While the use of a particular tropopause definition will inevitably introduce some uncertainty, this has been shown to be relatively small (~5%) for both column ozone [*Young et al.*, 2013] and tropospheric ozone RF [*Stevenson et al.*, 2013].

2.1. Tropospheric Emission Spectrometer

The Tropospheric Emission Spectrometer (TES) is an infrared Fourier transform spectrometer onboard NASA's Aura satellite, which was launched in 2004. In "Global Survey" operating mode (the data used in this study) TES makes nadir observations of the atmospheric ozone profile with a $5.3 \times 8.3\,\mathrm{km}$ footprint providing near-global coverage approximately every 16 days. TES ozone profiles have been extensively validated against in situ observations [*Nassar et al.*, 2008; *Osterman et al.*, 2008; *Richards et al.*, 2008], showing that TES has a small high bias of up to 15%. We use TES observations from July 2005 until June 2008.

2.2. TOMCAT

TOMCAT is a three-dimensional global chemical transport model [*Arnold et al.*, 2005; *Chipperfield*, 2006]. The version of the model used in this study contains a detailed chemical scheme optimized for the study of tropospheric composition [*Richards et al.*, 2013; *Monks et al.*, 2015]. Model simulations are performed at $\sim 2.8° \times 2.8°$ horizontal resolution, with 31 hybrid σ-p levels extending from the surface to 10 hPa and are forced using European Centre for Medium-Range Weather Forecasts (ECMWF) ERA-Interim temperature, winds, and humidity. Anthropogenic emissions are taken from the IPCC Fifth Assessment Report year 2000 emission set [*Lamarque et al.*, 2010]. PD biomass burning and natural wildfire emissions are prescribed from the Global Fire Emissions Database v2 [*van der Werf et al.*, 2006; *Randerson et al.*, 2007] yearly varying monthly mean estimates. Natural isoprene and monoterpene emissions were calculated off-line by the Model of Emissions of Gases and Aerosols from Nature as implemented by *Emmons et al.* [2010]. Other natural emissions are prescribed off-line from the POET data set [*Granier et al.*, 2005].

In order to compare TOMCAT with the TES observations, we performed a 4 year TOMCAT PD simulation using 2005–2008 meteorological data and the PD emissions described above. Global model fields of ozone were output every 6 h from July 2005 onward, with the profiles closest (both spatially and temporally) to each of the TES observations being selected for comparison. We also performed two additional 1 year simulations (using 2008 meteorological data, with a 6 month spin-up) where all anthropogenic emissions were omitted: TOMCAT PI, with historical biomass burning emissions for the year 1900 based on the Global Inventory for Chemistry-Climate Studies inventory [*Mieville et al.*, 2010], and TOMCAT PI (PD_BB), with PD biomass burning emissions.

2.3. The Radiative Transfer Model

Ozone REs are calculated using the off-line version of the *Edwards and Slingo* [1996] radiative transfer model and a methodology described in previous studies [*Riese et al.*, 2012; *Bekki et al.*, 2013; *Richards et al.*, 2013]. The radiative transfer model has six bands in the SW and nine bands in the LW, with a delta-Eddington two-stream scattering solver at all wavelengths. We employed a monthly mean climatology for water vapor and temperature based on ECMWF reanalysis data, surface albedo and cloud fields from year 2000 International Satellite Cloud Climatology Project data [*Rossow and Schiffer*, 1999], while aerosols have been ignored. The stratospherically adjusted REs were calculated using the fixed dynamic heating (FDH) approximation [*Fels et al.*, 1980]. As discussed by previous studies [e.g., *Forster and Shine*, 1997; *Maycock et al.*, 2011], the FDH method assumes that on relatively short time scales (typically less than 2 months) the atmosphere balances an initial heating rate perturbation through radiative processes only, without considering the associated dynamical feedbacks. This is implemented in the model by iteratively adjusting

Tropospheric O$_3$ RK [mWm^{-2} / ppbv / 100 hPa]
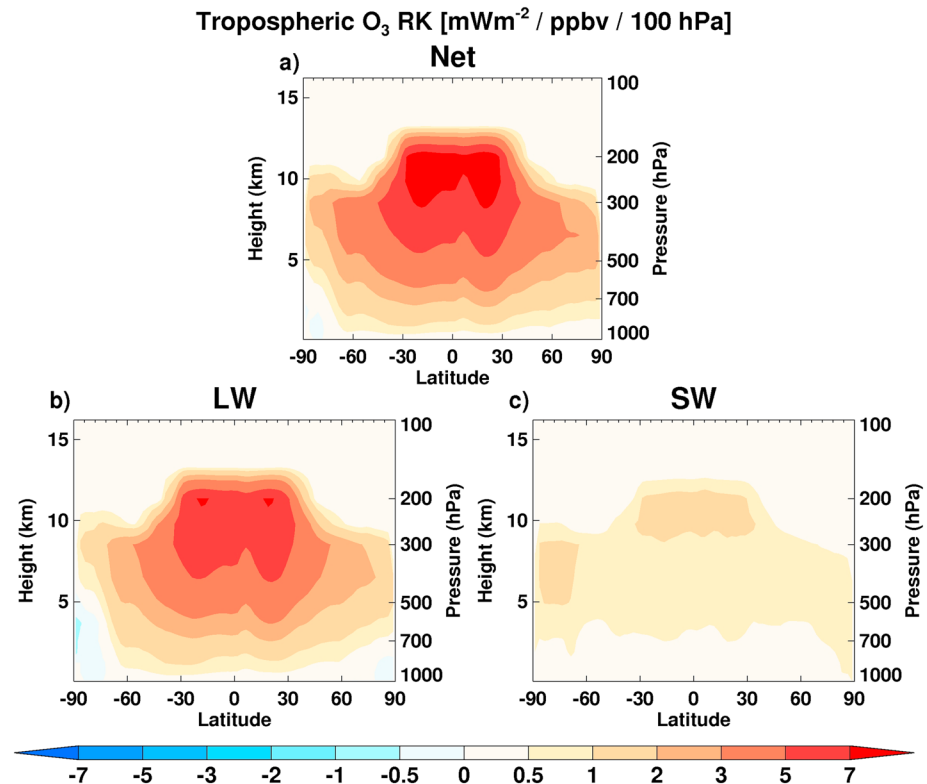
Figure 1. Annual zonal mean tropospheric ozone radiative kernel under all-sky conditions in units of mW m^{-2}/ppbv/100 hPa for (a) net (LW + SW), (b) LW, and (c) SW.

stratospheric temperatures (to account in our case for the heating rate imbalance caused by the tropospheric ozone change) until the stratosphere converges to radiative equilibrium.

We performed 10 radiative transfer simulations corresponding to different monthly mean 3-D tropospheric ozone profiles. Three of these simulations employ TES ozone measurements: (i) TES 05/06, using measurements from July 2005 to June 2006; (ii) TES 06/07 (July 2006 to June 2007); and (iii) TES 07/08 (July 2007 to June 2008). Three simulations employ TOMCAT-derived ozone profiles: (iv) TOMCAT PI, using historical biomass burning and no anthropogenic emissions; (v) TOMCAT PI (BB_PD) using PD biomass burning and no anthropogenic emissions; and (vi) TOMCAT PD, using present-day biomass burning and anthropogenic emissions. Three additional simulations employ ozone profiles obtained from applying the three annual TES averaging kernels to the TOMCAT PD output following the method of *Rodgers and Connor* [2003]: (vii) TOMCAT-AK 05/06, (viii) TOMCAT-AK 06/07, and (ix) TOMCAT-AK 07/08. These correspond to what the TES instrument would retrieve if observing TOMCAT PD ozone concentrations. While the TOMCAT PI and PD simulations can be used to estimate the tropospheric ozone RF, the TOMCAT-AK simulations are directly comparable with the three TES simulations to estimate differences between model and observations. Finally, tropospheric ozone REs for the above nine simulations were calculated by comparing against a zero tropospheric ozone simulation: (x) NO OZONE.

3. Results and Discussion

To illustrate our radiative transfer model's RE sensitivity to changes in tropospheric ozone, we use the *Soden et al.* [2008] radiative kernel (RK) concept, i.e., the derivative of the radiative flux with respect to perturbations in a particular atmospheric variable. This is obtained by performing calculations of stratospherically adjusted tropospheric ozone REs at the tropopause caused by 1 ppbv perturbations to the reference ozone climatology (in our case TOMCAT PD), applied successively to each model layer within the troposphere, while leaving concentrations at other grid points unchanged. Figure 1, which shows the tropospheric ozone RK in units of mW m^{-2}/ppbv/100 hPa, confirms the importance of the tropical tropopause region
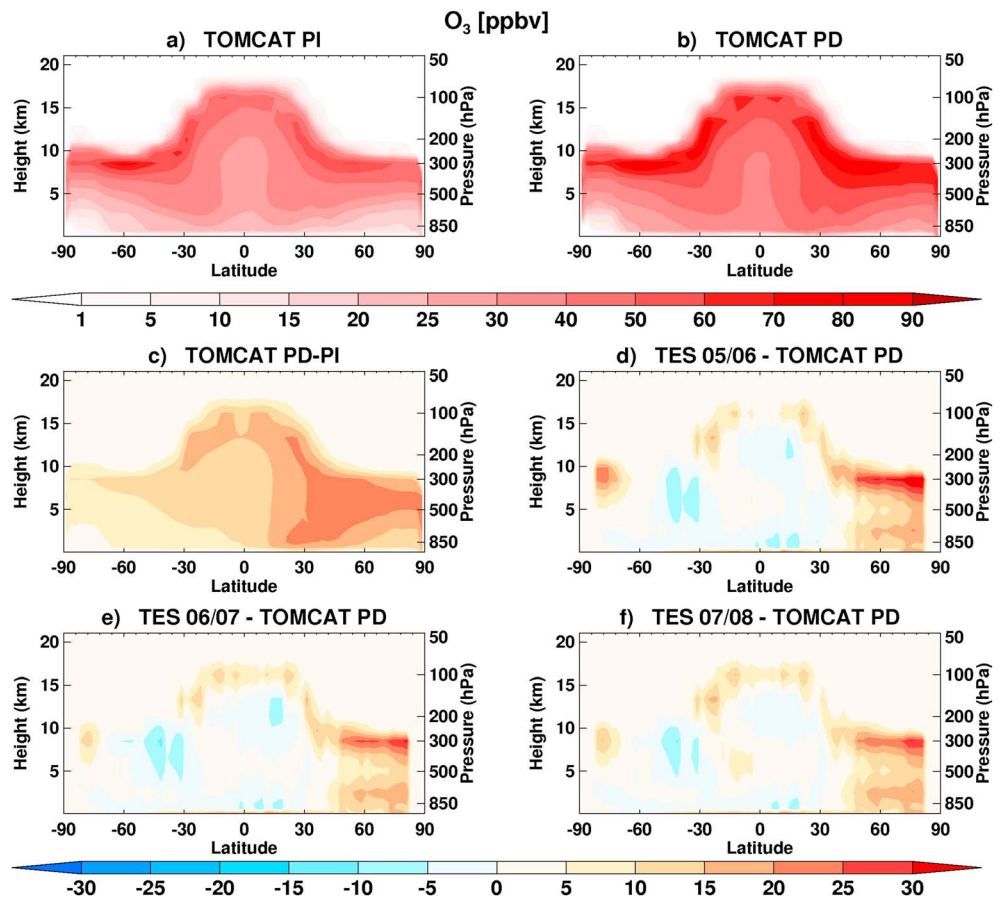
Figure 2. Annual zonal mean tropospheric ozone distributions (ppbv) for (a) TOMCAT PI, (b) TOMCAT PD, (c) TOMCAT PD–PI, (d) TES 05/06–TOMCAT PD, (e) TES 06/07–TOMCAT PD, and (f) TES 07/08–TOMCAT PD.

[*Worden et al.*, 2011; *Riese et al.*, 2012], where ozone changes are up to 10 times more efficient in altering the Earth's radiative flux than other regions. The RK is dominated by its LW component (Figure 1b), with a smaller SW component (Figure 1c) contribution. As we show later, the RK can be used as an accurate, computationally efficient tool for tropospheric ozone RE calculations, by simply multiplying it with 3-D (longitude × latitude × altitude) ozone profiles.

We note that the magnitude of our RK is substantially larger (a factor of ~10) than that of the *Worden et al.* [2011] instantaneous RKs. A large part of this difference is due to the fact that our RK includes both the LW and SW components and that it corresponds to the stratospherically adjusted RE at the tropopause, while the *Worden et al.* [2011] instantaneous RKs are based on the instantaneous TOA LW radiative flux. However, even when comparing similar quantities, i.e., LW component of the TOA instantaneous RK (Figure S1b in the supporting information), we still find that our values are a factor of ~3 larger than those from *Worden et al.* [2011]. While the different methodologies (e.g., cloud treatment) and radiative transfer methods (i.e., band model versus line-by-line model) are likely to be an important contributing factor, a future intercomparison study should try to fully understand these differences.

Figures 2a and 2b show TOMCAT PI and PD annual zonal mean tropospheric ozone. The largest PD ozone concentrations occur in the extratropical upper troposphere (up to 80 ppbv), followed by the northern hemisphere (NH) lower troposphere and the tropical upper troposphere (50–60 ppbv). This in good agreement with the ensemble mean results of 3-D models in the Atmospheric Chemistry and Climate Model Intercomparison Project (ACCMIP) [*Young et al.*, 2013]. For different latitudinal bands, the TOMCAT PD tropospheric ozone column is (ACCMIP mean and standard deviation is shown in brackets) 25.8 Dobson units (DU, 1 DU = 2.7×10^{16} molecules cm^{-2}) (25.7 ± 3.7) for 60°S–30°S, 29.0 DU (27.8 ± 3.4) for 30°S–equator,

Table 1. Annual Global Mean Tropospheric Ozone Column, Radiative Effects (REs) and Normalized Radiative Effects by Column Ozone (NREs) for the Radiative Transfer Model Simulations[a]

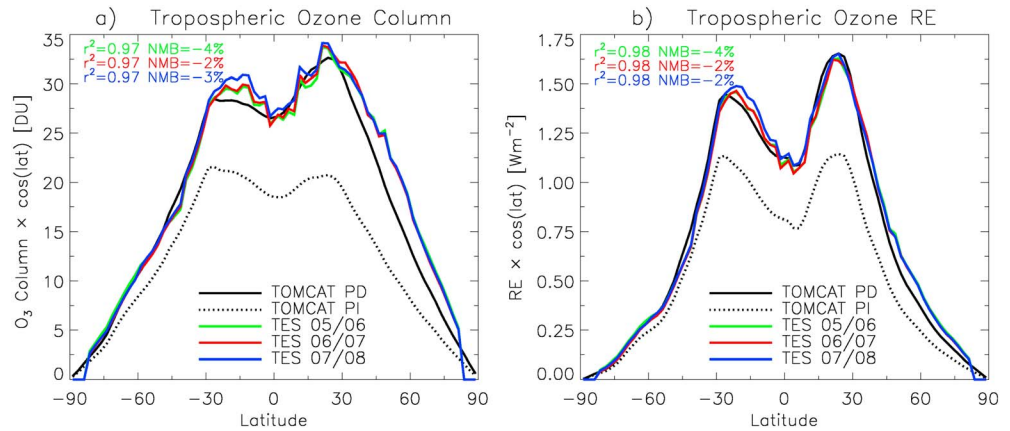|	Tropospheric O_3 Column (DU)	Tropospheric O_3 RE (W m^{-2})			NRE (mW m^{-2} DU^{-1})
		LW	**SW**	**Net**	
TOMCAT PI	19.7	0.70	0.15	0.85 (0.82)	43
TOMCAT PI (BB_PD)	21.6	0.77	0.17	0.94 (0.92)	43
TOMCAT PD	28.5	0.96	0.21	1.17 (1.16)	41
TOMCAT-AK 05/06	28.7	0.93	0.21	1.14 (1.15)	40
TOMCAT-AK 06/07	29.0	0.94	0.21	1.15 (1.15)	40
TOMCAT-AK 07/08	29.3	0.96	0.21	1.17 (1.17)	40
TES 05/06	29.9	0.97	0.21	1.18 (1.18)	39
TES 06/07	29.9	0.96	0.21	1.18 (1.17)	39
TES 07/08	30.4	0.98	0.22	1.20 (1.20)	39

[a]RE and NRE values are calculated using the radiation model by comparison against the NO OZONE simulation. Values in brackets are calculated using the radiative kernel (RK) technique, by multiplying the ozone profile fields with the RK.

31.5 DU (31.8 ± 2.7) for equator–30 N, and 34.8 DU (38.8 ± 4.1) for 30°N–60°N. Compared to PI values, we find that ozone concentrations in the PD are larger across all altitudes and latitudes with maximum increases (up to 25 ppbv) in northern midlatitudes and high latitudes (Figure 2c), which is again consistent with the ACCMIP results [*Young et al.*, 2013].

Figures 2d–2f show zonal mean differences between 3 years of TES satellite measurements and the TOMCAT PD zonal mean tropospheric ozone. Previous studies have shown that TES tropospheric ozone retrievals have a high bias of approximately 10 ppbv compared to aircraft data [*Richards et al.*, 2008] and ozonesondes [*Nassar et al.*, 2008]. We also find differences between the TES observations and the TOMCAT simulated concentrations in several regions, with TES observed concentrations smaller (by up to 10 ppbv) than the model in tropical and southern hemisphere (SH) midlatitude regions and larger (by up to 30 ppbv) in NH midlatitudes and high latitudes, especially in the upper troposphere. Previous studies recorded biases of similar magnitude between TES tropospheric ozone concentrations and global chemistry-climate models [*Aghedo et al.*, 2011; *Bowman et al.*, 2013]. In terms of tropospheric ozone column, the agreement between TES and TOMCAT is generally good, as at some latitudes biases at different levels tend to compensate each other. From Table 1, the annual global mean tropospheric ozone column from TES varies between 29.9 and 30.4 DU, while the corresponding TOMCAT-AK values vary between 28.7 and 29.3 DU, all within the ACCMIP range of 30.8 ± 2.7 DU [*Young et al.*, 2013]. The largest differences in column ozone occur in the SH tropical and NH midlatitude and high latitude regions where TES values for all 3 years are larger than the corresponding model results (Figure 3a).

We calculate the tropospheric ozone RE for all simulations using our radiative transfer model and the fixed dynamic heating approximation [*Fels et al.*, 1980]. The global mean tropospheric ozone REs for the three TES simulations are in the range of 1.18–1.20 W m^{-2}, with the corresponding TOMCAT-AK values at 1.14–1.17 W m^{-2} (Table 1). Together with the REs calculated using our radiative transfer model, Table 1 also shows that the RK technique can be used to provide very good net RE estimates (shown in brackets). While the good agreement between the observed and the modeled ozone columns (Figure 3a) does not necessarily imply the same for their REs [*Lacis et al.*, 1990; *Bowman et al.*, 2013], Figure 3b shows that there is indeed a remarkable agreement between the modeled and observed annual zonal mean REs. This is caused by the fact that the largest differences in ozone concentration occur mainly in regions where the RE sensitivity to ozone is relatively small (i.e., NH midlatitudes and high latitudes; Figures 2d–2f) compared to more RE-sensitive regions such as the tropical tropopause (Figure 1).

Our results therefore indicate that in terms of radiative effect the TOMCAT PD tropospheric ozone is well constrained, and consequently, an annual global mean tropospheric ozone RE of 1.17 ± 0.03 W m^{-2} appears robust. According to our model, this is the result of a dominant LW effect (0.95 ± 0.02 W m^{-2}) but also a nonnegligible SW effect (0.21 ± 0.01 W m^{-2}) which accounts for almost 20% of the net RE (Table 1). We also find that the RE normalized by the column ozone (NRE) decreases from 43 mW m^{-2} DU^{-1} in the PI simulations to 39 mW m^{-2} DU^{-1} in the PD simulations (Table 1). This is caused by the fact that the largest
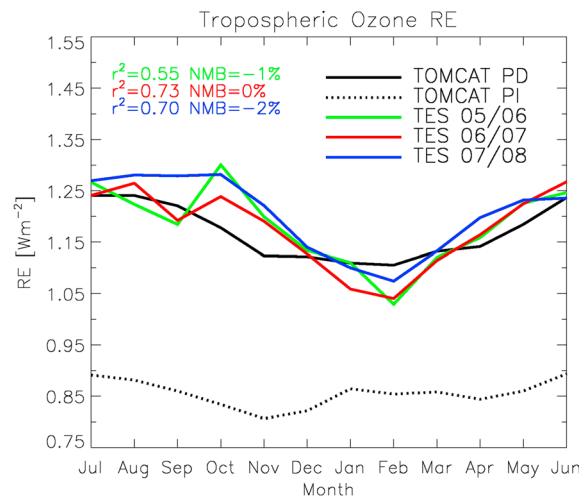
Figure 3. Annual zonal mean values of tropospheric ozone (a) column (DU) and (b) radiative effect (Wm^{-2}) from TOMCAT and TES. The values are weighted by cos(latitude) for a better comparison of how different latitude bands contribute to the global mean. Coefficients of determination r^2 and normalized mean bias (NMB) for the three sets of annual mean 2-D (longitude × latitude) TOMCAT-AK versus TES (a) ozone column and (b) ozone radiative effect are also shown.

tropospheric ozone increases between PI and PD occur outside the peak regions of RE sensitivity to ozone (tropical upper troposphere as shown by Figure 1), such as the NH midlatitudes below 500 hPa (Figure 2c).

Throughout the year the seasonal cycle of the global mean tropospheric ozone RE is determined by the ozone seasonal cycle and varies between a boreal winter minimum and a boreal summer maximum (Figure 4). For the TOMCAT PD and the three TES simulations, the December-January-February means are 1.11 W m^{-2} and 1.08–1.10 W m^{-2}, while the June-July-August means are 1.24 W m^{-2} and 1.25–1.26 W m^{-2}, respectively. As shown by Figure 4, while there is a larger monthly variation in the TES simulations compared to the TOMCAT PD simulation, they are in good overall agreement, with only a very small TOMCAT PD low bias (normalized mean bias NMB between −2% and 0%).

Allowing for stratospheric temperatures to adjust has a substantial effect on the calculated tropospheric ozone RE, as it changes its LW component (it reduces the LW component at the tropopause and increases it at TOA). The annual global mean IREs (i.e., before stratospheric adjustment) at TOA and tropopause in our model are 0.68 W m^{-2} (LW 0.47 W m^{-2}; SW 0.21 W m^{-2}) and 1.36 W m^{-2} (LW 1.15 W m^{-2}; SW 0.21 W m^{-2}), respectively. Thus, there is a factor of 3 difference between the net IRE at the tropopause and the LW IRE at TOA, which partly explains the large difference between the only two existing tropospheric ozone IRE estimates. Our RE values are in-between these two other estimates, being ~10% smaller than the *Joiner et al.* [2009] IRE at the tropopause for January and July 2005 of 1.53 W m^{-2} (our corresponding value being 1.37 W m^{-2}) and ~45% larger than the *Worden et al.* [2011] LW IRE at TOA for August 2006 of 0.33 W m^{-2} (our corresponding value being 0.48 W m^{-2}).

Taking the difference between the REs calculated in the TOMCAT PD and PI simulations (Table 1), we estimate the tropospheric ozone RF to be 0.32 W m^{-2}, which is within the 5–95% confidence IPCC [*Myhre et al.*, 2013] and the ±1 standard deviation ACCMIP [*Stevenson et al.*, 2013]

Figure 4. Monthly global mean tropospheric ozone radiative effect (Wm^{-2}) from TOMCAT and TES. Coefficients of determination r^2 and normalized mean bias NMB of TOMCAT PD versus TES monthly global mean ozone radiative effect are also shown.

ranges of 0.2–0.6 W m^{-2} and 0.41 ± 0.12 W m^{-2}, respectively. As noted by previous studies, the main source of uncertainty in these RF estimates comes from the poorly constrained PI ozone levels. In our study we highlight this uncertainty by considering the additional TOMCAT PI (BB_PD) simulation, where PI biomass burning emissions are assumed to be the same as those in the PD. With this assumption, the estimated RF is reduced by almost 30% to 0.23 W m^{-2} compared to the case when historical biomass burning emissions are considered. Thus, despite the well-constrained radiative effect of tropospheric ozone in the PD, the poorly constrained historical biomass burning emissions lead to substantial RF uncertainty. The NRE decrease between the PI and the PD results in the normalized RF (NRF), estimated here at 36 mW m^{-2} DU^{-1}, being smaller than the NRE. This NRF dependence on the background ozone abundance is supported by previous studies, which recorded larger multimodel mean NRFs between PI and PD (42 mW m^{-2} DU^{-1}) [*Stevenson et al.*, 2013] than between PD and 2100 (36 mW m^{-2} DU^{-1}) [*Gauss et al.*, 2003].

Finally, we propose the use of model radiative kernels as an efficient and accurate tool for calculating tropospheric ozone REs and RFs, particularly suitable for large model intercomparison studies. Once a radiative kernel is constructed (Figure 1), this can be multiplied by tropospheric ozone distributions to obtain associated REs (kernel available on request from the corresponding author). Table 1 indicates that the REs calculated using this radiative kernel technique (shown in brackets) are in very good agreement with corresponding values calculated using our radiation model. While the error introduced by this technique is very small for all our PD simulations, it is important to note that due to the decrease in NRE between the PI and the PD simulations, the error increases for PI simulations, suggesting that different model radiative kernels should be used for very different ozone abundances.

References

Aghedo, A. M., K. W. Bowman, H. M. Worden, S. S. Kulawik, D. T. Shindell, J. F. Lamarque, G. Faluvegi, M. Parrington, D. B. A. Jones, and S. Rast (2011), The vertical distribution of ozone instantaneous radiative forcing from satellite and chemistry climate models, *J. Geophys. Res.*, *116*, D01305, doi:10.1029/2010JD014243.

Arnold, S. R., M. P. Chipperfield, and M. A. Blitz (2005), A three-dimensional model study of the effect of new temperature-dependent quantum yields for acetone photolysis, *J. Geophys. Res.*, *110*, D22305, doi:10.1029/2005JD005998.

Bekki, S., A. Rap, V. Poulain, S. Dhomse, M. Marchand, F. Lefevre, P. M. Forster, S. Szopa, and M. P. Chipperfield (2013), Climate impact of stratospheric ozone recovery, *Geophys. Res. Lett.*, *40*, 2796–2800, doi:10.1002/grl.50358.

Boucher, O., and D. Tanré (2000), Estimation of the aerosol perturbation to the Earth's radiative budget over oceans using POLDER satellite aerosol retrievals, *Geophys. Res. Lett.*, *27*(8), 1103–1106, doi:10.1029/1999GL010963.

Bowman, K. W., et al. (2013), Evaluation of ACCMIP outgoing longwave radiation from tropospheric ozone using TES satellite observations, *Atmos. Chem. Phys.*, *13*(8), 4057–4072, doi:10.5194/acp-13-4057-2013.

Chipperfield, M. P. (2006), New version of the TOMCAT/SLIMCAT off-line chemical transport model: Intercomparison of stratospheric tracer experiments, *Q. J. R. Meteorol. Soc.*, *132*(617), 1179–1203, doi:10.1256/qj.05.51.

Edwards, J. M., and A. Slingo (1996), Studies with a flexible new radiation code. 1. Choosing a configuration for a large-scale model, *Q. J. R. Meteorol. Soc.*, *122*(531), 689–719, doi:10.1002/qj.49712253107.

Emmons, L. K., et al. (2010), Description and evaluation of the Model for Ozone and Related chemical Tracers, version 4 (MOZART-4), *Geosci. Model Dev.*, *3*(1), 43–67.

Fels, S. B., J. D. Mahlman, M. D. Schwarzkopf, and R. W. Sinclair (1980), Stratospheric sensitivity to perturbations in ozone and carbon-dioxide: Radiative and dynamical response, *J. Atmos. Sci.*, *37*(10), 2265–2297, doi:10.1175/1520-0469(1980)037<2265:sstpio>2.0.co;2.

Forster, P. M., and K. P. Shine (1997), Radiative forcing and temperature trends from stratospheric ozone changes, *J. Geophys. Res.*, *102*(D9), 10,841–10,855, doi:10.1029/96JD03510.

Forster, P., et al. (2007), Changes in atmospheric constituents and in radiative forcing, in *Climate Change 2007: The Physical Science Basis. Contribution of Working Group I to the 4th Assessment Report of the Intergovernmental Panel on Climate Change*, edited by S. Solomon et al., pp. 129–234, Cambridge Univ. Press, Cambridge, U. K., and New York.

Gauss, M., et al. (2003), Radiative forcing in the 21st century due to ozone changes in the troposphere and the lower stratosphere, *J. Geophys. Res.*, *108*(D9), 4292, doi:10.1029/2002JD002624.

Granier, C., J. F. Lamarque, A. Mieville, J. F. Muller, J. Olivier, J. Orlando, J. Peters, G. Petron, G. Tyndall, and S. Wallens (2005), POET, a database of surface emissions of ozone precursors.

Heald, C. L., D. A. Ridley, J. H. Kroll, S. R. H. Barrett, K. E. Cady-Pereira, M. J. Alvarado, and C. D. Holmes (2014), Contrasting the direct radiative effect and direct radiative forcing of aerosols, *Atmos. Chem. Phys.*, *14*(11), 5513–5527, doi:10.5194/acp-14-5513-2014.

Joiner, J., M. R. Schoeberl, A. P. Vasilkov, L. Oreopoulos, S. Platnick, N. J. Livesey, and P. F. Levelt (2009), Accurate satellite-derived estimates of the tropospheric ozone impact on the global radiation budget, *Atmos. Chem. Phys.*, *9*(13), 4447–4465.

Lacis, A. A., D. J. Wuebbles, and J. A. Logan (1990), Radiative forcing Of climate by changes in the vertical-distribution of ozone, *J. Geophys. Res.*, *95*(D7), 9971–9981, doi:10.1029/JD095iD07p09971.

Lamarque, J. F., et al. (2010), Historical (1850–2000) gridded anthropogenic and biomass burning emissions of reactive gases and aerosols: Methodology and application, *Atmos. Chem. Phys.*, *10*(15), 7017–7039, doi:10.5194/acp-10-7017-2010.

Lelieveld, J., and F. J. Dentener (2000), What controls tropospheric ozone?, *J. Geophys. Res.*, *105*(D3), 3531–3551, doi:10.1029/1999JD901011.

Maycock, A. C., K. P. Shine, and M. M. Joshi (2011), The temperature response to stratospheric water vapour changes, *Q. J. R. Meteorol. Soc.*, *137*, 1070–1082, doi:10.1002/qj.822.

Mieville, A., C. Granier, C. Liousse, B. Guillaume, F. Mouillot, J. F. Lamarque, J. M. Grégoire, and G. Pétron (2010), Emissions of gases and particles from biomass burning during the 20th century using satellite data and an historical reconstruction, *Atmos. Environ.*, *44*(11), 1469–1477, doi:10.1016/j.atmosenv.2010.01.011.

Monks, S. A., et al. (2015), Multi-model study of chemical and physical controls on transport of anthropogenic and biomass burning pollution to the Arctic, *Atmos. Chem. Phys.*, *15*, 3575–3603, doi:10.5194/acp-15-3575-2015.

Myhre, G., et al. (2013), Anthropogenic and natural radiative forcing, in *Climate Change 2013: The Physical Science Basis. Contribution of Working Group I to the Fifth Assessment Report of the Intergovernmental Panel on Climate Change*, edited by T. F. Stocker et al., pp. 659–740, Cambridge Univ. Press, Cambridge, U. K., and New York.

Nassar, R., et al. (2008), Validation of Tropospheric Emission Spectrometer (TES) nadir ozone profiles using ozonesonde measurements, *J. Geophys. Res.*, *113*, D15S17, doi:10.1029/2007JD008819.

Osterman, G. B., et al. (2008), Validation of Tropospheric Emission Spectrometer (TES) measurements of the total, stratospheric, and tropospheric column abundance of ozone, *J. Geophys. Res.*, *113*, D15S16, doi:10.1029/2007JD008801.

Randerson, J. T., van der Werf, G. R., Giglio, L., Collatz, G. J., Kasibhatla, P. S. (2007), Global Fire Emissions Database, version 2 (GFEDv2.1), Data Set. [Available at http://daac.ornl.gov/.] Oak Ridge National Laboratory Distributed Active Archive Center, Oak Ridge, Tenn., doi:10.3334/ORNLDAAC/849.

Rap, A., C. E. Scott, D. V. Spracklen, N. Bellouin, P. M. Forster, K. S. Carslaw, A. Schmidt, and G. Mann (2013), Natural aerosol direct and indirect radiative effects, *Geophys. Res. Lett.*, *40*, 3297–3301, doi:10.1002/grl.50441.

Richards, N. A. D., G. B. Osterman, E. V. Browell, J. W. Hair, M. Avery, and Q. B. Li (2008), Validation of Tropospheric Emission Spectrometer ozone profiles with aircraft observations during the intercontinental chemical transport experiment-B, *J. Geophys. Res.*, *113*, D16S29, doi:10.1029/2007JD008815.

Richards, N. A. D., S. R. Arnold, M. P. Chipperfield, G. Miles, A. Rap, R. Siddans, S. A. Monks, and M. J. Hollaway (2013), The Mediterranean summertime ozone maximum: global emission sensitivities and radiative impacts, *Atmos. Chem. Phys.*, *13*(5), 2331–2345, doi:10.5194/acp-13-2331-2013.

Riese, M., F. Ploeger, A. Rap, B. Vogel, P. Konopka, M. Dameris, and P. Forster (2012), Impact of uncertainties in atmospheric mixing on simulated UTLS composition and related radiative effects, *J. Geophys. Res.*, *117*, D16305, doi:10.1029/2012JD017751.

Rodgers, C. D., and B. J. Connor (2003), Intercomparison of remote sounding instruments, *J. Geophys. Res.*, *108*(D3), 4116, doi:10.1029/2002JD002299.

Rossow, W. B., and R. A. Schiffer (1999), Advances in understanding clouds from ISCCP, *Bull. Am. Meteorol. Soc.*, *80*(11), 2261–2287, doi:10.1175/1520-0477(1999)080<2261:aiucfi>2.0.co;2.

Soden, B. J., I. M. Held, R. Colman, K. M. Shell, J. T. Kiehl, and C. A. Shields (2008), Quantifying climate feedbacks using radiative kernels, *J. Clim.*, *21*(14), 3504–3520, doi:10.1175/2007jcli2110.1.

Stevenson, D. S., et al. (2013), Tropospheric ozone changes, radiative forcing and attribution to emissions in the Atmospheric Chemistry and Climate Model Intercomparison Project (ACCMIP), *Atmos. Chem. Phys.*, *13*(6), 3063–3085, doi:10.5194/acp-13-3063-2013.

van der Werf, G. R., J. T. Randerson, L. Giglio, G. J. Collatz, P. S. Kasibhatla, and A. F. Arellano (2006), Interannual variability in global biomass burning emissions from 1997 to 2004, *Atmos. Chem. Phys.*, *6*, 3423–3441.

Worden, H. M., K. W. Bowman, S. S. Kulawik, and A. M. Aghedo (2011), Sensitivity of outgoing longwave radiative flux to the global vertical distribution of ozone characterized by instantaneous radiative kernels from Aura-TES, *J. Geophys. Res.*, *116*, D14115, doi:10.1029/2010JD015101.

Young, P. J., et al. (2013), Preindustrial to end 21st century projections of tropospheric ozone from the Atmospheric Chemistry and Climate Model Intercomparison Project (ACCMIP), *Atmos. Chem. Phys.*, *13*(4), 2063–2090, doi:10.5194/acp-13-2063-2013.